Proc. VIIth Digital Image Computing: Techniques and Applications, Sun C., Talbot H., Ourselin S. and Adriaansen T. (Eds.), 10-12 Dec. 2003, Sydney

Mapping Between Digital and Continuous Projections via the Discrete Radon Transform in Fourier Space

Andrew Kingston and Imants Svalbe

Center for X-ray Physics and Imaging,
School of Physics and Materials Engineering,
Monash University, VIC 3800, Australia.
andrew.kingston@spme.monash.edu.au

Abstract. This paper seeks to extend the Fourier space properties of the discrete Radon transform, $R(t, m)$, proposed by Matus and Flusser in [1], to expanded discrete projections, $R(k, \theta)$, where the wrapping of rays is removed. This expanded mode yields projections more akin to the continuous space sinogram. It is similar to the Mojette transform defined in [2], but has a pre-determined set of discrete projection angles derived from the Farey series [3]. It is demonstrated that a close approximation to the sinogram of an image can be obtained from $R(k, \theta)$, both in Radon and Fourier space. This investigation is undertaken to explore the possibilities of applying this mapping to the inverse problem, that of obtaining discrete projection data from continuous projection data as a means of efficient tomographic reconstruction that requires minimal interpolation and filtering.

Keywords: discrete Radon transform, tomographic image reconstruction, discrete Fourier slice theorem.

1 Introduction

The discrete Radon transform (DRT) is a mapping of data from a 2-D discrete function, $I(x, y)$, to a set of 1-D discrete projections. Beylkin first defined the class of transforms termed DRTs in 1987 [4]. This paper investigates two of the transforms in this class and makes comparisons in both Radon and Fourier space with a more continuous form of the RT, the sinogram. The DRT applied here is the $R(t, m)$ mapping proposed by Matus and Flusser in [1] and an expanded version of this, $R(k, \theta)$ first described by Svalbe in [5, 6] and subsequently developed in [7]. Discrete projection transforms may enable images to be reconstructed from real projection data with fewer free parameters than current tomographic techniques, yielding higher fidelity reconstructed images with fewer reconstruction artifacts.

Fig. 1 depicts the various transforms explored here and their relationship to two well-established tomographic methods, Fourier inversion (FI) and filtered back-projection (FBP). FI involves 2-D interpolation of the radial slices obtained

from the 1-D DFT of the continuous projections, $\widehat{\Re}(\rho,\theta)$ onto a Cartesian grid, $\widehat{I}(u,v)$ and applying the inverse 2-D DFT to obtain the image, $I(x,y)$ [11]. This method produces artifacts in the reconstructed image due to the interpolation, particularly at edges. FBP applies a selected filter to the projections in Fourier space to effectively differentiate the projection data, this produces artifacts in the image reconstructed through the inverse of the projection process[11]. Reconstructing discrete images from discrete projections is an exact process therefore errors only occur in the mapping from continuous to discrete projection data. This mapping is the topic of this paper. The broader aim is to explore the possibility of improving the quality of tomographic reconstruction using the DRT.

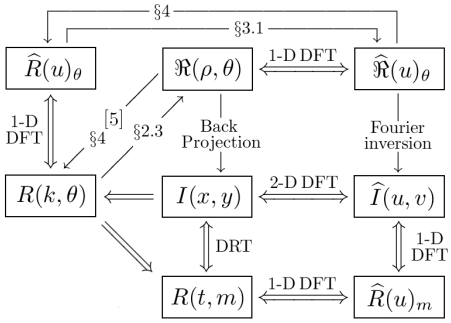

Fig. 1. Relationship between the discrete transforms as defined in this paper. $\Leftrightarrow$ represents an exact, invertible 1:1 mapping, $\Rightarrow$ represents an exact mapping in one direction only, $\rightarrow$ represents an approximate mapping requiring some form of interpolation or filtering.

$R(t,m)$ is defined on arrays of prime (p) size under modulo p arithmetic. Digital projections are a set of discrete sums along lines $x = my + t \bmod p$ for all intercepts $0 \leq t < p$ at some gradient m, $0 \leq m \leq p$. Due to the modulo p arithmetic, lines are wrapped around the image (refer Fig. 2a). A similar DRT which can be applied to arrays of size 2^n as well as prime size arrays is proposed in [8]. The transform $R(k,\theta)$ is obtained by separating these wrapped ray-sums with intercepts t, into individual ray-sums with intercepts $k_{ty_m}, k_{ty_m \pm p}, k_{ty_m \pm 2p}, \ldots$ This expanded mode can be viewed as a discrete form of the continuous sinogram, $\Re(\rho,\theta)$. It is similar to the Mojette transform defined in [2] however with a predetermined angle set. The discrete angle set common to $R(t,m)$ and $R(k,\theta)$ is found to be a subset of the Farey series [3].

Whilst these discrete ray-sums are useful in digital applications [9, 10], they do not have a direct connection to projections in the physical world. This paper demonstrates two methods of forward mapping from discrete projections, $R(k,\theta)$ of an image to a set of continuous projections, $\Re(\rho,\theta)$, one method in Radon

Space (§2.3) and another in Fourier space (§3.1). In [5] it was shown $R(k,\theta)$ can be used to reconstruct an image from $\Re(\rho,\theta)$ via the inverse of the mapping described in §2.3, using linear interpolation. Results were significantly improved when images were reconstructed at large p and sub-sampled to the required size. This improvement was ascribed to the reduction of relative gap size between the discrete ray sample points, d_m (refer Fig. 2a). $d_{\max}$, the upper limit for d_m in the DRT angle set for an image of size p, scales with $\sqrt{p}$. Discrete projections with large d_m are shown to be important in §3.2 as they contain much of the high frequency information. In this paper, the properties of $R(k,\theta)$ in Fourier space are explored to develop a new method to achieve the inverse mapping, obtaining discrete projections from continuous projections acquired at the DRT angle set via the inverse of the mapping described in §3.1 without requiring the case of large p image size.

The notation for the 1-D and 2-D discrete Fourier transforms (DFT) used in this paper, as well as the sinogram and its properties in Fourier Space is as follows. Let $\widehat{I}_y(u)$, $0 \le u < p$, be the 1-D DFT of row y of a 2-D $p \times p$ discrete function, $I(x,y)$, found as

$$\widehat{I}_y(u) = \sum_{x=0}^{p-1} I(x,y) \exp[-i2\pi ux/p]. \tag{1}$$

Let $\widehat{I}(u,v)$ be the 2-D DFT of $I(x,y)$, found as

$$\widehat{I}(u,v) = \sum_{x=0}^{p-1}\sum_{y=0}^{p-1} I(x,y) \exp[-i2\pi(ux+vy)/p] \tag{2}$$

In Fourier space, the spatial frequency f is given by u in $\widehat{I}(u)_y$ and by the distance from the origin in $\widehat{I}(u,v)$, i.e., $\sqrt{u^2+v^2}$. The spatial wavelength corresponding to f is p/f.

The sinogram, $\Re(\rho,\theta)$, of a continuous 2-D function, $f(x,y)$, obtained from the real world can be thought of as a set of p unit-width ray-integrals with intercepts ρ, $\lfloor -p/2 \rfloor \le \rho \le \lfloor p/2 \rfloor$, over an imaging circle of diameter p at a discrete set of angles, θ [11]. It is depicted in Fig. 2c and has the form

$$\Re(\rho,\theta) = \int_{-\infty}^{\infty} f(\rho\sin\theta + s\cos\theta, -\rho\cos\theta + s\sin\theta)ds. \tag{3}$$

The Fourier slice theorem states that the 1-D Fourier transform of a projection at angle θ is equivalent to a central radial slice through the 2-D Fourier transform of the original object/function at the angle $\theta^{\perp} = \theta + \pi/2$ [11]. For a discrete set of intercepts, ρ, this is approximated by $\widehat{\Re}_\theta(u) = \widehat{f}(u\sin\theta, -u\cos\theta)$, $\lfloor -p/2 \rfloor \le \rho \le \lfloor p/2 \rfloor$ [11]. Fig. 5c shows the distribution in Fourier space of one projection of $f(x,y)$ of size $p = 29$ at the angle shown in Fig. 2c. The next section defines the digital projections that characterise the DRT.

2 Discrete Radon Transform Projections

2.1 $R(t, m)$

$R(t, m)$, as defined by Matus and Flusser [1], replaces the continuous integrals of (3) with discrete sums along the line $x = my + t \bmod p$. As with the 2-D DFT, it assumes the image is periodic over size p, thus the digital rays wrap around the image under modulo p arithmetic. The DRT, as depicted in Fig. 2a for $p = 29$, $t = 0$, $m = 9$, is defined as

$$R(t,m) = \begin{cases} \sum_{x=0}^{p-1} I(x,t) & : \quad m = 0, \\ \sum_{y=0}^{p-1} I(\langle my + t \rangle_{\text{mod } p}, y) & : \quad 0 < m \leq p. \end{cases} \tag{4}$$

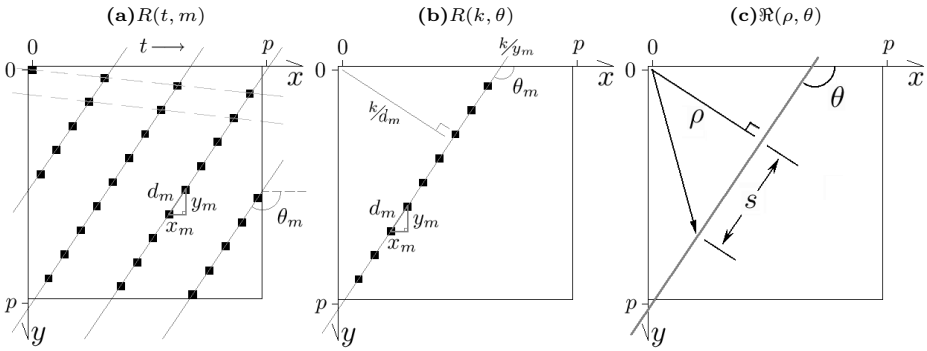

Fig. 2. (a) Sample pattern of one $R(t, m)$ raysum, $t = 0$ and $m = 9$ for $p = 29$. Black squares represent pixels sampled by the ray-sum. Dashed line represents line $x = my + t \bmod p$ for generation of the sampling pattern. Solid lines represent the resulting projection direction giving minimum gap distance between adjacent sampled pixels. Here $x_9 = -2$,$y_9 = 3$ hence $d_9^2 = 13$ and $\theta_9 = \tan^{-1}(3/-2)$. **(b)** Sample pattern for one $R(k, \theta)$ raysum at θ_9 with $k = t + 2p = 58$. **(c)** Depiction of one line integral in $\Re(\rho, \theta)$, as defined in (3).

2.2 $R(k, \theta)$

For a given m, as defined in §2.1, the pixels of the image that are sampled to form a discrete ray-sum are depicted in Fig. 2a. d_m is defined as the minimum gap distance between samples along a discrete modulo p ray with a separation distance x_m in the horizontal and y_m in the vertical, giving $d_m^2 = x_m^2 + y_m^2$. The angle of d_m defines the projection angle $\theta_m = tan^{-1}(y_m/x_m)$. It was shown in [3] that for the DRT angle set, $1 \leq d_m^2 \leq d_{\max}^2 = 2p/\sqrt{3}$.

$R(k,\theta)$ is found by separating the wrapped digital rays, m, into individual digital rays, labelled by translates k, at angle θ_m (Fig. 2b). $R(k,\theta)$ has the same sampling pattern as $R(t,m)$ defined by x_m and y_m with ray-sums found as

$$R(k,\theta) = \sum_{x=0}^{p-1}\sum_{y=0}^{p-1} I(x,y)\delta_0(k - xy_m + yx_m), \tag{5}$$

where the delta function, $\delta_0(x)$, is 1 when $x = 0$ and equals 0 otherwise. The number of discrete ray-sums in each projection, N_m, is not constant. There are py_m rays for $0 \le x \le p$ and $p|x_m|$ rays from $0 \le y \le p$, therefore $N_m = p(|x_m| + y_m) = pw_m$ [5]. Each row of $R(k,\theta)$ has period N_m.

2.3 Sinogram from $R(k,\theta)$ in Radon Space

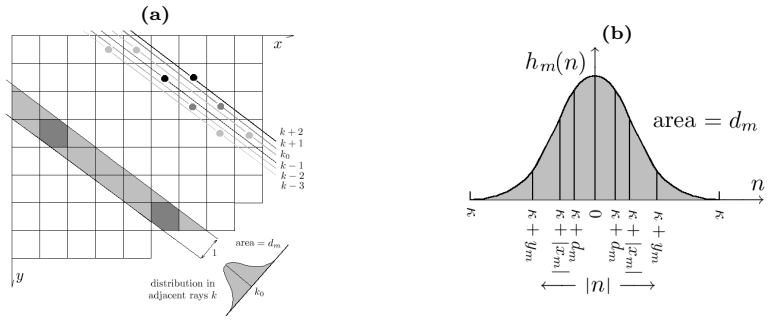

Fig. 3. (a) Depiction of a unit width ray-integral comprised of overlapped adjacent discrete projections at some k_0, shown for a projection angle $\tan^{-1}(3/4)$. The dark grey pixels correspond to the central digital projection, k_0 with contribution to the unit width ray-integral $h_m(0)$. **(b)** general form of ray-spread function $h_m(n)$ defined in (6), where n is distance from the central digital ray, k_0. Depicts contribution to the unit width ray-integral from the digital projections neighbouring k_0.

The sinogram of an image with each projection sampled at a discrete set of angles can be obtained by convolving $R(k,\theta)$ with a ray-spread function, $h_m(n)$ (Fig. 3), defined for the case where $|x_m| \le y_m$, by

$$h_m(n) = \begin{cases} 1 - \frac{w_m - d_m}{2(w_m + d_m)} - \frac{2n^2}{2|x_m|y_m} & : \quad 0 \le |n| \le \kappa - d_m \\ 1 - \frac{w_m - d_m + 4n}{4(w_m + d_m)} - \frac{n^2}{2|x_m|y_m} & : \quad \kappa - d_m \le |n| \le \kappa - |x_m| \\ \frac{y_m}{w_m - d_m} + \frac{2n - y_m}{2|x_m|y_m} & : \quad \kappa - |x_m| \le |n| \le \kappa - y_m \\ \frac{w_m + d_m + 4n}{4(w_m - d_m)} + \frac{n^2}{2|x_m|y_m} & : \quad \kappa - y_m \le |n| \le \kappa \\ 0 & : \quad |n| \ge \kappa, \end{cases} \tag{6}$$

where $n = k_0 - k$ and $\kappa = (w_m + d_m)/2$ for $w_m = |x_m| + y_m$[12]. For the case of $|x_m| > y_m$, y_m and x_m are exchanged in (6). This function describes

the distribution of a continuous ray-integral, of unit-width, centred on k_0 by the overlap of 2κ adjacent discrete rays. The contribution of each k to the ray-integral is determined by the proportion of area of the pixels sampled by the unit-width ray. $h_m(n)$ is applied at p locations, k_0, in each digital projection (separated by intervals of d_m) found as $k_0 = \lfloor p/2 \rfloor (y_m - x_m) \pm \eta d_m$ for $0 \leq \eta \leq \lfloor p/2 \rfloor$. The distance d_m in discrete projection space at angle, θ corresponds to a unit distance perpendicular to θ in image space, i.e., $\rho = kd_m$ in Fig. 2. Therefore at all angles, θ, the central pd_m elements in the discrete projection define an imaging circle of diameter p in image space. Fig. 4 shows an example of a continuous sinogram obtained from a discrete image using (6). The resulting sinogram has the same angle set as the DRT. As a subset of the Farey series, it is based on equi-spaced gradients rather than equi-spaced angles, giving rise to the apparent discontinuities at $\pi/4, \pi/2$ and $3\pi/4$. Fig. 7a gives an example of the distribution of projection angles in the DRT for $p = 29$. This gives an approximation to the

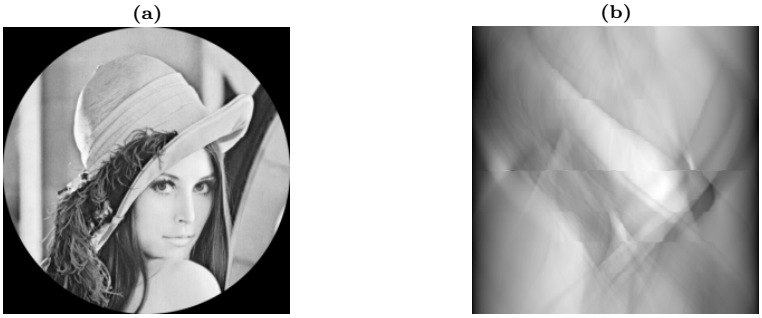

Fig. 4. (a) 257 × 257 image I(x,y). **(b)** 257 × 258 sinogram resulting from the convolution of R with h_m described in §2.3. This produces p unit width ray-integrals at the $p + 1$ DRT angles.

sinogram that would be obtained as projections of a real object or continuous function at the DRT angle set. The sinogram can be treated as a sample of the discrete convolution $\widehat{R} * \widehat{h}$. To reconstruct the image from the sinogram, the inverse of this convolution must be performed to obtain the discrete transform.

3 Fourier Analysis of $R(t, m)$ and $R(k, \theta)$

Since there is a mapping between discrete and continuous projections in Radon space, there should be some form of discrete Fourier Slice theorem for $R(k, \theta)$. It was shown in [1] that the elements of the DFT of a projection, m, produced in $R(t, m)$ correspond to elements in the 2-D Fourier space according to

$$\widehat{R}_m(u) = \begin{cases} \widehat{I}(0, u) & : \quad m = 0, \\ \widehat{I}(u, \langle -mu \rangle_{\text{mod } p}) & : \quad 0 < m \leq p. \end{cases} \tag{7}$$

There is a similar relationship for $R(k,\theta)$. As each projection is periodic over length N_m, the elements of the 1-D DFT of a (k,θ) projection correspond to elements in the 2-D Fourier space according to

$$\begin{aligned}\widehat{R}_\theta(u) &= \sum_{k=0}^{N_m-1}\sum_{x=0}^{p-1}\sum_{y=0}^{p-1} I(x,y)\exp[-i2\pi uk/N_m]\delta_0(k-x_m y+yx_m) \qquad (8)\\ &= \sum_{x=0}^{p-1}\sum_{y=0}^{p-1} I(x,y)\exp[-i2\pi(uy_m x-ux_m y)/N_m]\\ &= \widehat{I}(\frac{y_m}{w_m}u,-\frac{x_m}{w_m}u) \bmod p,\ 0\le u<N_m.\end{aligned}$$

This result has properties from both $\widehat{\Re}_\theta(u)$ and $\widehat{R}_m(u)$. It has a similar form to $\widehat{\Re}_\theta(u)$, since $y_m = d_m\sin\theta$ and $x_m = d_m\cos\theta$, i.e., $\widehat{R}_\theta(u) = \widehat{I}(\gamma\sin\theta,-\gamma\cos\theta)$ where $\gamma = \frac{d_m}{w_m}u$. The wrapped rays in Fourier space coincide with those for $\widehat{R}_m(u)$, as can be seen in Fig. 5.

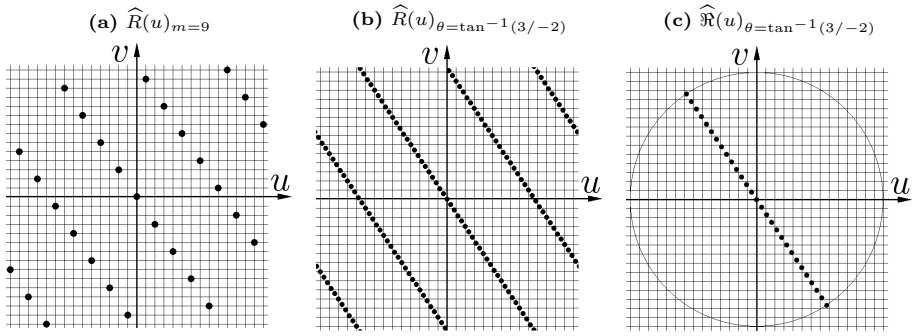

Fig. 5. Distribution of the DFT of the three different projections in 2-D Fourier Space. Projections are at $\tan^{-1}(3/-2)$ degrees (or gradient $m=9$) for an image of size $p=29$ as shown in Fig. 2. **(a)** the p spatial frequencies of the $R(t,m)$ projection. **(b)** the $N_m = pw_m = 145$ frequencies of the $R(k,\theta)$ projection. **(c)** the p frequencies of the $\Re(\rho,\theta)$ projection.

3.1 Sinogram from $R(k,\theta)$ in Fourier Space

The sinogram can also be obtained from $R(k,\theta)$ in Fourier space. From the discrete Fourier slice theorem, the p frequencies of $\widehat{\Re}_\theta(r)$ are separated by unit distance in the direction $\theta_m^\perp$ (Fig. 5c). The elements of $\widehat{R}_\theta(u)$ are separated by a distance d_m/w_m also in the direction $\theta_m^\perp$ (Fig. 5b). The principle difference is that $\widehat{R}_\theta(u)$ extends to a radius of pd_m and therefore must wrap in Fourier space since the 2-D DFT is modulo p in the x and y directions. Therefore the

relative magnitudes of r and u are given by $u = rd_m/w_m$. The first pd_m/w_m frequencies of $\widehat{R}_\theta(u)$ (i.e., out to a frequency of p), interpolated to be spanned by p frequencies gives $\widehat{\Re}_\theta(r)$.

3.2 DRT as a Frequency Filter

The discrete Fourier slice theorem for $R(t, m)$ defined in (7), implies that the DRT can serve as a crude frequency filter. The sampling pattern of the DRT for a ray-sum in $R(t, m)$ defined in (4) is identical but perpendicular to its DFT in 2-D Fourier space. Therefore, the projection sample gap distance, d_m, also gives the distance from the origin of frequencies sampled by that discrete projection in 2-D Fourier space, i.e., the minimum spatial frequency for that projection. The projection with $d_m = d_{\max}$ has a lower spatial frequency cut-off at $f = \sqrt{(2p/\sqrt{3})}$ [3]. Fig. 6a shows the distribution of projection samples in 2-D

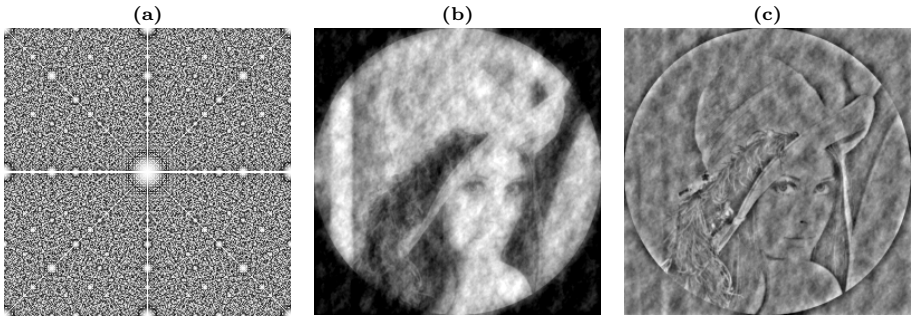

Fig. 6. (a) $R(t, m)$ projection distribution in 2-D Fourier Space for $p = 257$ (origin in centre of image). Grey levels for each digital projection are proportional to d_m, with white/(black) corresponding to $d_m = 1/(d_m = d_{\max})$. **(b)/(c)** images obtained by reconstructing image using projections where d_m is greater/less than $\sqrt{p/2\sqrt{3}}$.

Fourier Space. It can be seen that the projections with low d_m contain all the low frequency information. Fig. 6b and 6c demonstrate the DRT acting as a low and high pass filter. Fig. 6b was achieved by reconstructing $I(x, y)$ from $R(t, m)$ using only projections with $d_m < d_{\max}/2$ whilst in 6c only projections with $d_m > d_{\max}/2$ were used. This demonstrates that digital projections with large d_m are important in image reconstruction, as they contain more of the higher spatial frequency information as conjectured in [5]. When all digital projections are used, the frequency space is uniformly sampled and the reconstruction is exact.

4 Reconstruction of Images

Reconstructing images from continuous projection data via the DRT requires the inverse mapping to that of obtaining the sinogram via $R(k, \theta)$ described

in §2.3 and §3.1. The method presented here involves interpolation from the Fourier transform $\widehat{\Re}(u_\rho)_\theta$ to $\widehat{R}(u_k)_\theta$. This uses the DFT data from all sinogram projections to obtain the frequencies of each individual discrete projection (Fig. 7a). Previous methods have expanded the p elements from just one continuous projection into $N_m = pw_m$ elements via linear interpolation [5, 13] or matrix methods [12] using no information from projections at other angles (result for [5] in Fig. 7b). As more interpolation is required for large w_m (hence large d_m), the errors in the reconstructed image occur at higher frequencies. Interpolation

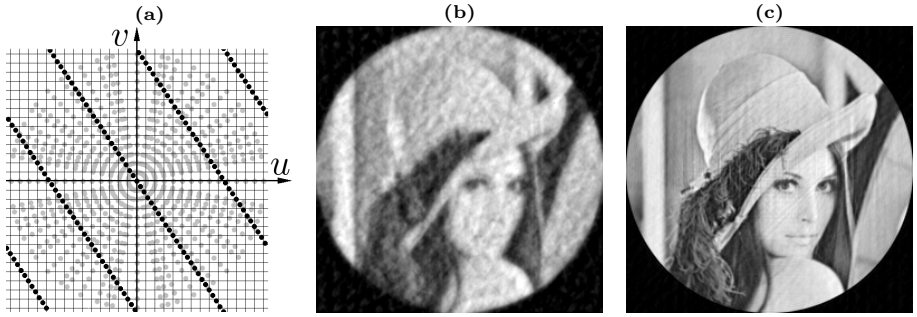

Fig. 7. (a) Illustrates the additional information obtained from the other projections for interpolation in Fourier space. Black dots represent elements of $\widehat{R}_\theta(u)$ that are required, grey dots represent data acquired from $\widehat{\Re}_\theta(u)$. **(b)** 257 × 257 image reconstructed from the 257 × 258 sinogram (Fig. 4b) via linear interpolation in (k, θ)-space. **(c)** Image reconstructed from sinogram via interpolation in Fourier space as described in §4.

in Fourier space enables use of the information from projections with angles near $\theta_m^\perp$ to improve the interpolation at θ_m. This is essential for projections with large d_m. The principal pw_m/d_m elements for each projection can be obtained directly from the DFT of the continuous projection at that angle. The remaining wrapped digital rays can be found by interpolation using the other Fourier slices. Those projections with large d_m, have additional information from the other slices $\widehat{\Re}_\theta(r)$ because a larger d_m produces more wrapped rays crossing the slices in Fourier space (refer Fig. 7a).

5 Conclusions

The properties of the DRT in Fourier space for both $R(t, m)$ and $R(k, \theta)$ were investigated. It was found that the (t, m) transform behaves as a crude frequency filter, where projections with larger d_m contain more of the high frequency information and are therefore important in image reconstruction. It was shown that the sinogram of the image with the DRT angle set could be obtained from the (k, θ) transform in both Radon and Fourier space. Mapping the sinogram to

$R(k, \theta)$, i.e., continuous to discrete projections in Fourier space was presented as a new method to reconstruct images. This technique reduces the amount of interpolation required to obtain each digital projection, as it uses more information from the continuous projections for discrete rays with larger d_m. Effectively, this fills the gaps between discrete samples. Efficient algorithms for implementing the $R(k, \theta)$ method and a comparison of image quality with Fourier inversion and filtered back projection is the subject of ongoing work.

6 Acknowledgements

Andrew Kingston is a Monash University postgraduate student in receipt of an Australian Postgraduate Award from the Australian Government. Imants Svalbe is supported by the Centre for X-ray Physics and Imaging at Monash University.

References

1. Matus, F., and Flusser, J., Image Representation via a Finite Radon Transform, IEEE Transactions on Pattern Analysis and Machine Intelligence, vol. 15, no. 10, pp. 996-1106, 1993.
2. Guedon, JP. and Normand, N., The Mojette Transform: Applications in Image Analysis and Coding, SPIE - Int. Soc. Opt. Eng., vol 3024, no. 2, pp 873 - 884, 1997.
3. Svalbe, I. and Kingston, A., Farey Sequences and Discrete Radon Transform Projection Angles, IWCIA, Palermo, Italy, May 14-16, 2003.
4. Beylkin, G., Discrete Radon Transform, IEEE Trans. on Acoustics, Speech and Signal Processing, vol. ASSP-35, no. 2, pp. 162-172, 1987.
5. Svalbe, I. and van der Spek, D., Reconstruction of Tomographic Images Using Analog Projections and the Digital Radon Transform, Linear Algebra and its Applications, 339, pp 125 - 145, 2001.
6. Svalbe, I., Natural Representations of Straight Lines and the Hough Transform in Discrete Arrays, IEEE TPAMI, vol 11, no. 9, pp 941-950, 1989.
7. Kingston, A. and Svalbe, I., Adaptive Discrete Radon Transform for Greyscale Images, IWCIA, Palermo, Italy, May 14-16, 2003.
8. Lun, D., Hsung, T., Shen, T., Orthogonal Discrete Periodic Radon Transform. Part I: theory and realization, Signal Processing, vol 83, no. 5, pp 941-955, 2003.
9. Svalbe, I., Image Operations in Discrete Radon Space, APRS DICTA, Melbourne, Australia, Jan 21-22, pp 285-290, 2002.
10. Lun, D., Hsung, T., Shen, T., Orthogonal Discrete Periodic Radon Transform. Part II: applications, Signal Processing, vol 83, no. 5, pp 957-971, 2003.
11. Kak, A. and Slaney, M., Principles of Computerized Tomographic Imaging, IEEE Press, 1988.
12. Kingston, A., k-space Representation of the Discrete Radon Transform, PhD. Thesis, School of Physics and Materials Engineering, Monash University (in preparation) 2003.
13. Svalbe, I. and Kingston, A., Intertwined digital rays in discrete Radon projections pooled over adjacent prime sized arrays, to be presented at DGCI, Naples, Italy, Nov 19-21, 2003.